07

Inverse spin Hall effect in structures based on yttrium iron garnet films with reduced saturation magnetization

© M.E. Seleznev,[1,2] S.L. Vysotskii,[1,2] G.M. Amakhanov,[3] Yu.V. Nikulin[1,2]

1 Saratov Branch, Kotelnikov Institute of Radio Engineering and Electronics, Russian Academy of Sciences, Saratov, Russia
[2] Saratov National Research State University, Saratov, Russia
[3] Yuri Gagarin State Technical University of Saratov, Saratov, Russia
e-mail: vysotsl@gmail.com

Received July 21, 2025
Revised November 19, 2025
Accepted November 19, 2025

The generation of EMF by the mechanism of the inverse spin Hall effect in platinum films deposited on the surface of yttrium iron garnet films with different values of saturation magnetization $4\pi M = 1750-540$ G was investigated due to the substitution of Fe ions by non-magnetic Ga and Sc ions. For the geometry of propagation of surface magnetostatic waves, the values of the efficiency of spin pumping E, defined as the ratio of the EMF to the power of the magnetostatic wave, were compared. At the bias field H greater than the saturation magnetization field H_s, the values of E are E $6.5-1.44 \cdot 10^{-3}$ V/W in the structures based on films with $4\pi M = 1750-850$ G and $1.44-2.5 \cdot 10^{-3}$ V/W for films with $4\pi M = 565-540$ G. It is shown that the parameter of doped films determining the efficiency of the ISHE in the structures based on them can be the nonuniform exchange constant α, with $E \sim 1/\alpha$. At $H < H_s$, the efficiency of spin pumping is inferior to the case of $H > H_s$ by more than an order of magnitude and decreases with decreasing $4\pi M$.

Keywords: saturation magnetization, surface magnetostatic waves, inverse spin Hall effect.

DOI: 10.61011/TP.2026.03.63167.192-25

Introduction

Mutual transformation effects of spin current and carrier current in ferrite–heavy metal multilayer structures [1–15] are actively studied due to future development of spintronic components on their basis [16,17]. Experimental studies most often cover the structures consisting of yttrium-iron garnet (YIG) films, where spin wave (SW) decay is record small, and platinum film deposited on their surface. In such structures, when high-frequency resonant magnetization oscillations [1–6] or propagating spin waves [7–10] are excited in YIG film, spin current I_s through the YIG–platinum interface can induce generation via the inverse spin Hall effect (ISHE) [18] of the carrier current $\mathbf{I}_e$ in the platinum film [7]:

$$\mathbf{I}_e \propto |I_{s,n}| [\mathbf{n} \times \mathbf{m}], \quad (1)$$

where $\mathbf{n}$ and $\mathbf{m}$ are unit vectors along the normal to YIG film surface and magnetization vectors, respectively, $I_{s,n}$ is the spin current component along the normal $\mathbf{n}$. Experiments most often measure $U = I_e R$, where R is the platinum film resistance.

It should be noted that spin-dependent electron-magnon scattering forms the basis of the ISHE mechanism [19]. The number of scattering channels N, which is defined by the number of magnetic ions at the YIG–platinum interface per unit area of the structure, is a key factor affecting this process [20–22]. In doped YIG films with low magnetization, where a part of iron ions in the lattice are replaced by rare-earth metal ions, decrease in the spin current can be expected due to reduction of the number of scattering channels. Such effect has been detected in the study of a YIG film structure with $4\pi M = 550$ G in [23] at $H > H_s$, where H_s is the ferrite film saturation field, and in [24] at $H < H_s$, however, the form of dependence of ISHE on the degree of magnetic ion replacement in YIG (i.e. on magnetization $4\pi M$) hasn't been investigated.

The purpose of this study is to investigate the inverse spin Hall effect in YIG film structures with saturation magnetizations in the range of 1750–540 G with bias magnetic fields corresponding to both the saturated film state $H > H_s$ and to formation of a domain structure in the film at $H < H_s$. In addition, the behavior of dependence of the spin pumping efficiency on $4\pi M$ is discussed.

1. Test structures and measurement procedure

Structures were fabricated using YIG films grown via liquid-phase epitaxy on gadolinium-gallium garnet (GGG) substrates with the (111) crystallographic orientation and saturation magnetizations of 1750–540 G (see the Table). Reduction of $4\pi M$ was achieved via doping with Ga and Sc ions with various replacement degrees [25]. 12×6 mm waveguides were cut from films in such a way that the

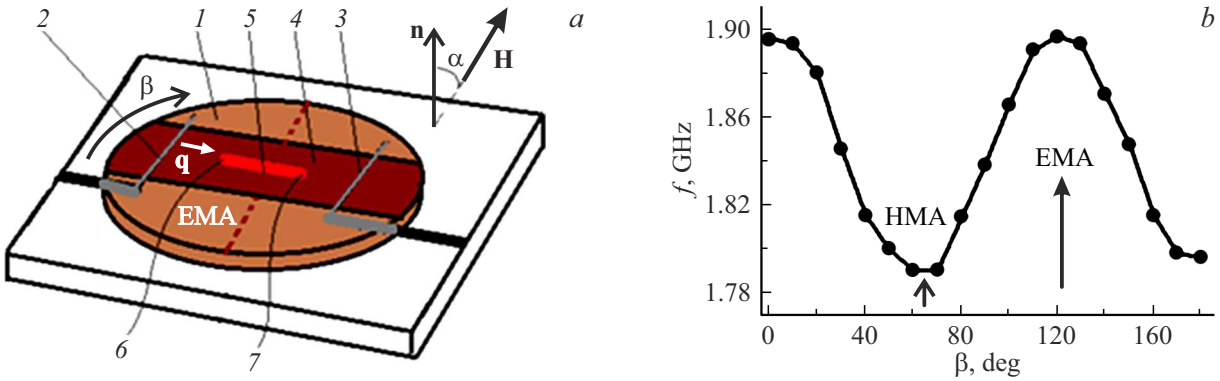

Figure 1. Schematic image of the MSSW delay line mockup used to determine the EMA direction and for measurements (a); $f_0(\beta)$ curve plotted for film № 4 at $H = 490$ Oe (b). Arrows correspond to the directions of H along the easy magnetization axis (EMA) and hard magnetization axis (HMA). White arrow shows the direction of the wave vector **q**.

$\langle 1\bar{1}0 \rangle$ easy magnetization axis (EMA) projection on the film plane is oriented along the short side. (In this case for measurements in a magnetostatic surface wave (MSSW) configuration, the generated EMF in the range of $H < H_s$ is the highest compared with other directions of **H** relative to the crystallographic axes of YIG films [26].)

EMA direction was determined in accordance with [27]. YIG film disc *1* (Figure 1, a) on the GGG substrate was laid over input microstrip antenna *2* and output microstrip antenna *3* and placed in the permanent magnetic field H tangent to the film surface (angle α between **H** and the normal to film surface **n** is 90°) parallel to the microstrip transducers. Such experimental configuration corresponds to MSSW distribution in YIG film. Long-wavelength boundary of the MSSW f_0 spectrum was determined. Then the mockup with antennas was turned in the electromagnet bore so that α was equal to approximately 45°. By turning the film on the microstrips towards β (Figure 1, a), curve $f_0(\beta)$ was built. Film orientation, at which f_0 reached its maximum was identified with magnetization along the EMA projection. Figure 1, b illustrates such dependence obtained for film № 4 from the table at $H = 490$ Oe. Waveguide *4* was cut from the test YIG disc in such a way that its long side is perpendicular to a particular EMA direction (Figure 1, a). Measurements were performed for all tested YIG films.

Parameters of test YIG films

№ film No.	d, μm	$4\pi M$, G	H_s, Oe	$E = U/P$, 10^{-3} V/W	H^*_{exp}, Oe	H^*_{calc}, Oe	α, 10^{-11} cm^2
1	15.6	1750	54	6.1	590	580	3.5
2	12	1750	60	6.5	600	580	3.5
3	15	1000	6	5.9	300	330	8
4	20	850	10	5.8	300	290	11
5	26	565	46	2.5	200	200	23
6	17	540	25	1.5	200	190	25

The waveguides were used for making YIG–Pt structures. Preparation for Pt deposition included chemical treatment of the YIG film surface (ultrasonic bath treatment in acetone; treatment in aqueous solution of nitric acid) followed by rinsing in deionized water in the ultrasonic bath. Immediately before Pt deposition, the film was degassed in vacuum $5 \cdot 10^{-6}$ Torr at ≈ 300 °C during 20 min. A Pt strip 4 nm in thickness, 4 mm in length and 25 μm in width was deposited along the long side of the waveguides using a magnetron sputtering mask technique. Wire contacts *6, 7* (Figure 1, a) to the strip for EMF measurement were made using conducting adhesive, strip resistance varied between samples within 5.5–8 kΩ.

After sputtering, the YIG–Pt structures were examined in the MSSW delay line (Figure 1, a at $\alpha = 90°$, the arrow shows the wave vector **q** direction) with microstrip antennas with a width of w$\approx 40\,\mu$m, spaced at 7 mm. The mockup was placed between the electromagnet poles and in a measurement module, for measurements at $H < H_s$, to allow additional detection of the type of domain structure (DS) using a polarization microscope coupled with a digital camera [28].

Frequency dependences of the modulus of transmission coefficient of the mockup $S(f)$ and power reflected from the input antenna $S_{ref}(f)$ were measured using the vector network analyzer at the generator output power P ranging from −30 to +10 dBm. Frequency dependences of EMF $U(f)$ were measured at $P = 10$ dBm. To increase the sensitivity of these measurements, synchronous detection method was used, for which microwave power was modulated by a 11.3 kHz square wave signal.

The following approach was used for comparing the spin pumping efficiency in structures with various YIG film properties. Inset in Figure 2, a shows typical frequency dependences $S(f)$ and $U(f)$. It can be seen that the maximum of $U(f)$ (with an asterisk) is observed near the low-frequency (long-wavelength) boundary f_0 of the

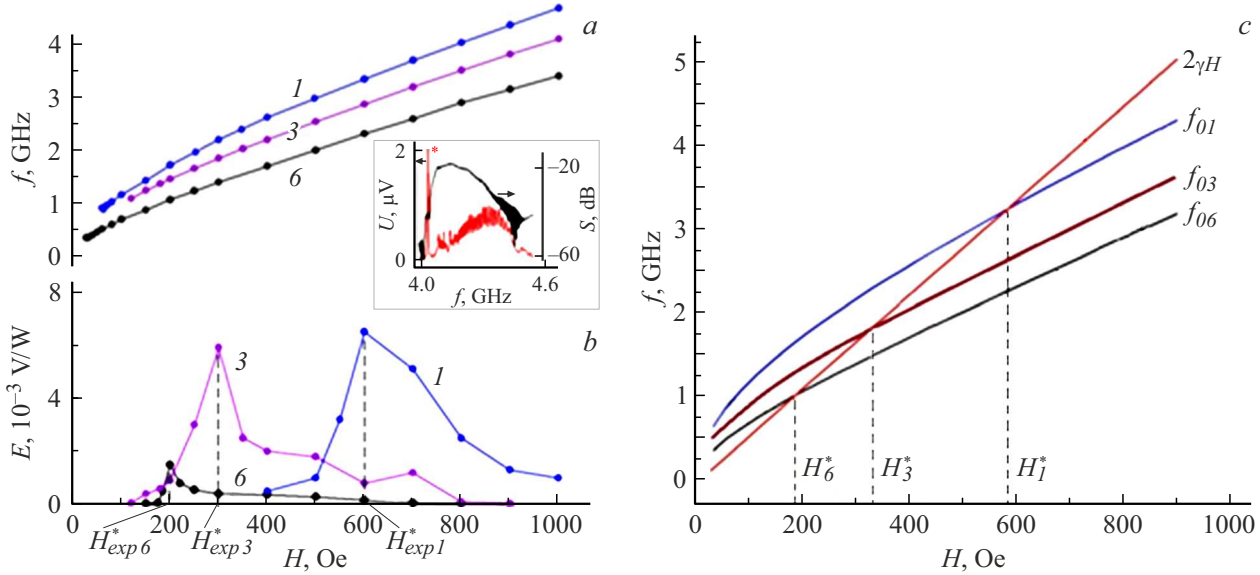

Figure 2. Dependences on the bias field H of the low-frequency (f_0) boundary of the MSSW existence region (a), and of the spin pumping efficiency (b) calculated using (2) the dependence on H of frequencies f_0 for structures № 1, № 3 and № 6 (c). Numbers on the curves and in indices correspond to structure numbers in the table.

MSSW spectrum [29]:

$$f_0 = \gamma\sqrt{H(H + 4\pi M)}, \qquad (2)$$

where γ is the gyromagnetic ratio, which is attributed to high density of magnon states caused by formation of the Van Hove singularity in this frequency region [30,31]. Frequency f_i corresponding to the highest value of U_i was measured for some value of the bias field H_i, then the MSSW power P_{swi} was calculated at this frequency as a difference of values of $S_{ref}(f)$ obtained at H_i and at $H \gg H_i$. When using the obtained values, the pumping efficiency (volt-watt sensitivity) was calculated as $E_i = U_i/P_{swi}$. Measurements were performed for a set of values of H from the range of 0−1 kOe. The data was used to build curve $E(H)$.

2. Measurements and discussion

2.1. $H > H_s$

We first consider the EMF generation for the case of YIG films magnetized to saturation. Figure 2 shows dependences on H of the long-wavelength boundaries of the MSSW observation region f_0 (Figure 2, a) and of the spin pumping efficiency E determined as described above (Figure 2, b) obtained experimentally for structures № 1, № 3 and № 6 Numbers on the curves correspond to structure (film) numbers in the table. Figure 2, b shows that all given curves $E(H)$ demonstrate maxima. The table shows maximum values of $E = U/P$ from the measurement range for each structure, and the corresponding values of the bias field H^*_{exp}. We discuss conditions that define the positions of these maxima.

Figure 2, c shows curves $f_0(H)$ calculated using (2) for structures № 1, № 3 and № 6, and curves $f = 2\gamma H$, where γ is the gyromagnetic ratio. It can be seen that positions of dashed lines corresponding to H^*_{exp} correlate well with H^*_{calc} calculated using (2), at which $f_{0i} \approx 2\gamma H$, where i is the structure number (Figure 2, b, c and the table listing the calculations for all structures).

We consider the influence of MSSW excitation and propagation conditions on the spin pumping efficiency. It is known that parametric instability processes displayed in the form of pumping spin wave decay into parametric spin waves (PSW) can develop in YIG films at MSSW power levels higher than a threshold value and when the laws of conservation of energy are obeyed

$$f_p = f_1 + f_2, \quad \mathbf{k} = \mathbf{k}_1 + \mathbf{k}_2,$$

where f_p and k are the pumping frequency and wave vector; $f_{1,2}$ and $\mathbf{k}_{1,2}$ are the PSW frequencies and wave numbers. Nonthreshold processes of PSW coalescence to form secondary spin waves (SSW) are also possible in turn [32,33]:

$$f_1 + f_2 = f_3, \quad \mathbf{k}_1 + \mathbf{k}_2 = \mathbf{k}_3,$$

where f_3 and $\mathbf{k}_3$ are the SSW frequency and wave vector.

Analysis of ISHE in YIG−Pt structures in parametric instability conditions has detected an effect of spin current generation acceleration due to three-magnon decays, that occurred when a maximum was observed on $U\big(f_0(H)\big)$ [34–36] and was attributed to the transfer of angular momentum from the lattice to magnetic system [34–36], and to the influence of PSW on the magnetization relaxation rate in magnetic film [35,36]. However, it was shown in [37]

that this effect could be explained by the fact that the electron-magnon scattering process involved SSW formed in nonthreshold PSW coalescence processes [33]. We show that it is the reason why the above-mentioned maxima in $E(H)$ are observed in our measurements.

Figure 3 shows the signal spectra at the output antenna of the MSSW delay line mockup for structure № 6 with the fixed pumping frequency $f^* = 1.07$ GHz (shown in the figure) and MSSW power P higher than the threshold power for three-magnon decays P_{th} with supercriticality 25–30 dB. This frequency corresponds to $H = H^*_{\text{exp }6} = 200$ Oe in Figure 2, *b*. It can be seen that, besides f^*, the spectrum contains a noise signal in the Δf region (Figure 3) caused by occurrence of SSW. At $H = 200$ Oe, f^* falls within the Δf band (Figure 3, *b*), which allows SSW to populate a spectrum segment, increasing the density of magnon states at f_0 and, thus, facilitating the increase in EMF generation efficiency similar to [30]. At the same time at $H = 150$ Oe (Figure 3, *a*) and 210 Oe (Figure 3, *c*), noise signal frequency regions don't overlap the pumping frequency and don't contribute to the density of magnon states.

We discuss the behavior of the dependence of spin pumping efficiency on saturation magnetization of the test films as shown by curve *1* in Figure 4. It can be seen that the trend of this curve $E = E(4\pi M)$ considerably differs from line *2*, which was plotted on the assumption that the pumping efficiency decreases linearly from $6.5 \cdot 10^{-3}$ V/W at $4\pi M = 1750$ G to $E = 0$ at $4\pi M = 0$. Difference between dependences *1* and *2* is probably attributed to the fact that, in doped films, not only does the saturation

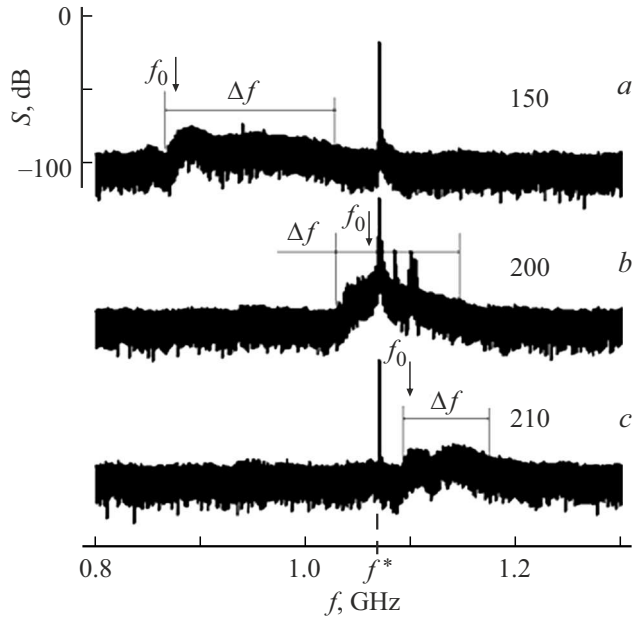

Figure 3. Frequency dependences of the signal spectrum at the output antenna of the MSSW delay line mockup for structure № 6 at the pumping frequency $f^* = 1.07$ GHz (marked with an asterisk in the figure). $H = 150$ (*a*), 200 (*b*), 210 Oe (*c*).

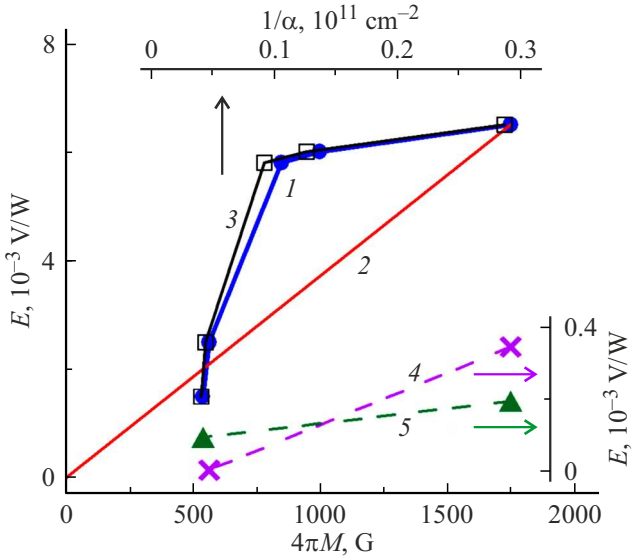

Figure 4. Dependences of experimental values of E on $4\pi M$ (curve *1*); dependence of E on $1/\alpha$ (curve *3*). Number *2* marks the simulated linear dependence $E = E(4\pi M)$. Dependences $E(4\pi M)$ for films № 2 (curve *4*) and № 6 (curve *5*) at $H < H_s$.

magnetization vary, but also do the exchange hardness A and related nonuniform exchange constant $\alpha = A/M^2$ [25]. We evaluate qualitatively the dependence of E on the YIG film properties. It was noted above that the generated EMF is proportional to the number of electron-magnon scattering channels ($N \sim M$). Scattering eficiency in each channel ρ depends on the density of inversely proportional to the group velocity of spin waves V_g [38]. $V_g(f)$ in turn is related to A and M as $V_g \sim A/M$ [29,39]. Thus, $E \sim N\rho \sim M^2/A \sim 1/\alpha$ can be expected.

Figure 4 shows the dependence of spin pumping efficiency E on $1/\alpha$ (curve *3*) plotted using α calculated similar to [25] for YIG films with various degrees of replacement by gallium and scandium (see the table). The scale and relative positions of the $4\pi M$ and $1/\alpha$ axes were selected so that to match the values of $4\pi M$ from the third column of the table for each film with the values of $1/\alpha$ calculated from the data in column 8 of the table. It can be seen that curves *1* and *3* almost coincide. Thus, it is suggested that α is an integrated parameter that takes into account the effect of doped YIG film properties on the ISHE efficiency.

2.2. $H < H_s$

We turn now to the results obtained with H reduced to $H < H_s$. For each film, this parameter was determined via decreasing H by a combination of attributes — variation of the course of field dependence of frequency boundaries of the MSSW observation region, occurrence of additional signal transmission regions in the MSSW spectrum, observation of DS using a polarization microscope. The obtained values of H_s are shown in the table. It can be seen that H_s

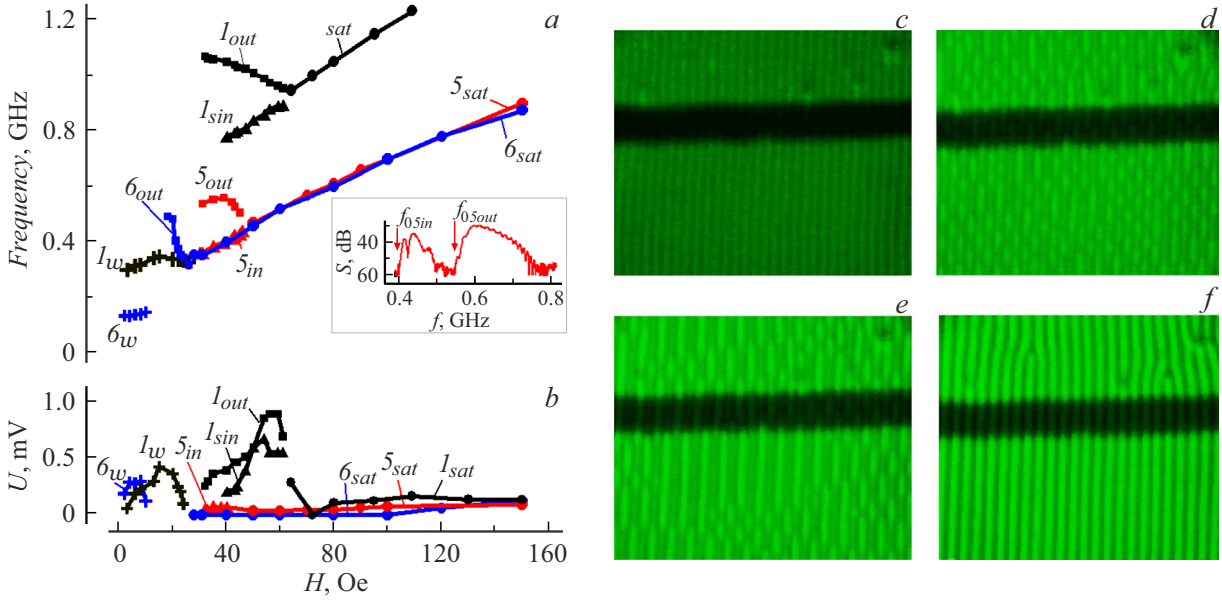

Figure 5. Dependences on the bias field of low-frequency boundaries of the exitance region of MSSW (curves with index „*sat*“), SWE induced by in-phase oscillations (curves with index „*in*“) and out-of-phase oscillations (curves with index „*out*“) of magnetization in domains, and SWE induced by domain boundary displacement waves (curves with index „*w*“) (*a*) and the corresponding dependences of EMF with the same marking (*b*) obtained for structures № 1, № 5 and № 6. Determination of f_{0in} and f_{0out}, $H = 40$ Oe is illustrated in the inset to the figure *a* using structure № 5 . Images of DS in structure № 5 at $H = 40$ (*c*), 27 (*d*), 24 (*e*) and 18 Oe (*f*). Dark Pt band in the figures is 25 μm in width.

in the normal magnetization films is 54–60 Oe. For films with low magnetization, H_s decreases, and the degree of reduction can be either low (film № 5) or drastic, where DS can be observed only at H on the order of several oersteds (film № 3).

Figure 5, *a* uses structure № 1 to illustrate the dependences on H of low-frequency boundaries of MSSW (curve *1 sat* (saturated)), in-phase (curve *1 in* (in-phase)) and out-of-phase (*1 out* (out of phase)) magnetization oscillations in domains, and of spin-wave excitation (SWE) induced by domain boundary displacement waves (curve *1 w*) [40,41]. For all SWE, EMF generation was detected (curves *1 sat*, *1 in*, *1 out*, *1 w* in Figure 5, *b*). Domain structure demonstrated good contrast and retained a strip form as H decreased to 0. These results are typical when using YIG films with normal magnetization with the (111) orientation [26,28].

For doped film structures, measurements differed qualitatively. Thus, in structures № 3, № 4 with $H_s = 6$–10 Oe, SWE couldn't be detected, and the domain structure had low contrast and was poorly defined.

Spectra of structures № 5 ($H_s = 46$ Oe) and № 6 ($H_s = 25$ Oe) contained SWE corresponding to out-of-phase magnetization oscillations in domains (curves *5 out*, *6 out* in Figure 5, *a*). In addition, for structure № 5 — SWE induced by in-phase magnetization oscillations in domains (curve *5 in* in Figure 5, *a*), and for № 6 — SWE induced by domain boundary displacement waves (curve *6 w* in Figure 5, *a*). Domain structure images had good contrast. In structure № 6, DS was observed at $H < 25$ Oe and retained a strip form with a period of about 10 μm as H decreased to 0. At the same time, rearrangement of the DS form in structure № 5 had particular features. It could be observed as H decreased to 40 Oe in the form of asymmetric strip DS with a period of 8 μm (Figure 5, *c*). Within $28 > H > 23$ Oe, DS took on a „dashed form“ — strip domains were broken into segments with different lengths (Figure 5, *e*). When H was rearranged, the form of DS varied (Figure 5, *e,d*), and at $H < 20$ Oe, DS took on a symmetric strip form with a period of 8 μm (Figure 5, *f*); such form of DS was maintained when H decreased to 0 with its period increased to 10 μm. Note that when „dashed“ DS was formed, SWE were not detected any longer and were not observed until H decreased to 0.

The described differences in domain structure formation conditions and rearrangement behavior during bias field variation are probably attributed to variations between films of both the uniaxial (growth) anisotropy and the anisotropy axis direction relative to the normal to the film surface described in [42] for YIG films with normal magnetization. The presence of dopants in the lattice of the test films with low magnetization can contribute to occurrence of additional features in the above-mentioned differences.

EMF generation in structure № 6 was observed only during excitation of the domain boundary displacement wave (curve *6 w* in Figure 5, *b*), while the spin pumping efficiency was equal to approximately $0.1 \cdot 10^{-3}$ V/W, which is comparable with the result of a similar calculation for

structure № 2 ($0.2 \cdot 10^{-3}$ V/W). In structure № 5, only for SWE induced by in-phase magnetization oscillations in domains, a weak EMF signal was detected (curve *5 in* in Figure 5, *b*), which corresponds to $E < 10^{-4}$ V/W. Note that, though the obtained data are insufficient to evaluate the form of dependence of pumping efficiency on the YIG film parameters, decrease in E as $4\pi M$ decreases agrees with results obtained for $H > H_s$.

Conclusion

The study has investigated the spin pumping efficiency E using the inverse spin Hall effect mechanism in YIG−Pt structures with MSSW propagating in them as the saturation magnetization of YIG film $4\pi M$ decreased from 1750 G to 540 G. It is shown that at the bias field $H > H_s$ for films with $4\pi M = 1000-850$ G, E is comparable with the case of film with normal magnetization and decreases by a factor of 2−3 for films with $4\pi M = 565-540$ G, while $E = E(4\pi M)$ differs from the linear dependence, and the form of dependence of E on the degree of doping can be described as $E \sim 1/\alpha$, where α is the nonuniform exchange constant of the film. Note that the maximum pumping efficiency for all test structures is observed with bias fields corresponding to the fulfilment of $f_{0i} \approx 2\gamma H$.

With $H < H_s$, EMF generation in doped film structures can be detected only for some SWE of domain structure, while the spin injection efficiency is twice as low as in the case of $4\pi M = 1750$ G, and the obtained values in absolute magnitude are lower than those of the saturated film case by more than an order of magnitude.

Funding

The study was supported by grant No. 24-29-00640 provided by the Russian Science Foundation.

Conflict of interest

The authors declare no conflict of interest.

References

[1] S.A. Manuilov, C. Du, R. Adur, H.L. Wang, V. Bhallamudi, F. Yang, P.C. Hammel. Appl. Phys. Lett., **107** (4), 042405 (2015). https://doi.org/10.1063/1.4927451.
[2] C.W. Sandweg, Y. Kajiwara, K. Ando, E. Saitoh, B. Hillebrands. Appl. Phys. Lett., **97** (25), 252504 (2010). https://doi.org/10.1063/1.3528207
[3] N.I. Polzikova, S.G. Alekseev, V.A. Luzanov, A.O. Raevskii. Phys. of the Solid State, **60** (11), 2211 (2018). DOI: 10.1134/S1063783418110252
[4] K.Y. Constantinian, G.A. Ovsyannikov, K.L. Stankevich, T.A. Shaikhulov, V.A. Shmakov, A.A. Klimov. Phys. of the Solid State, **63**, 1432 (2021). DOI: 10.1134/S1063783421090201
[5] M.B. Jungfleisch, A.V. Chumak, A. Kehlberger, V. Lauer, D.H. Kim, M.C. Onbasli, C.A. Ross, M. Klaui, B. Hillebrands. Phys. Rev. B., **91**, 134407 (2015). DOI: 10.1103/PhysRevB.91.134407
[6] S. Manna, R. Medwa, J.R. Mohan, S. Gupta, M.S. Sabir, J.V. Vas, H. Asada, Y. Fukuma, R.S. Rawat. Appl. Phys. Lett., **126**, 242407 (2025). DOI: 10.1063/5.0263385
[7] A.V. Chumak, A.A. Serga, M.B. Jungfleisch, R. Neb, D.A. Bozhko, V.S. Tiberkevich, B. Hillebrands. Appl. Phys. Lett., **100** (8), 082405 (2012). DOI: 10.1063/1.3689787
[8] J. Wang, H. Wang, J. Chen, W. Legrand, P. Chen, S.L. Heng, J. Xia, G. Lan, Y. Zhang, R. Yuan, J. Dong, X. Han, J.P. Ansermet, H. Yu. Phys. Rev. Appl., **21**, 044024 (2024). http://dx.doi.org/10.1103/PhysRevApplied.21.044024
[9] R.O. Serha, D.A. Bozhko, M. Agrawal, R.V. Verba, M. Kostylev, V.I. Vasyuchka, B. Hillebrands, A. Serga. Adv. Mater. Interf., **9**, 2201323 (2022). https://doi.org/10.1002/admi.202201323
[10] J. Wang, H. Wang, J. Chen, W. Legrand, P. Chen, L. Sheng, J. Xia, G. Lan, Y. Zhang, R. Yuan, J. Dong, X. Han, J.P. Ansermet, H. Yu. Phys. Rev. Appl., **21**, 044024 (2024). https://doi.org/10.1103/PhysRevApplied.21.044024
[11] F. Hou, M. Xu, X. Chen, Y. Dong, X. Han, T. Li, X. Wang, T. Min. Physica B: Cond. Matt., **695** (15), 416542 (2024). https://doi.org/10.1016/j.physb.2024.416542
[12] R. Kohno, N.M. Thiéry, K. An, P. Noël, L. Vila, V.V. Naletov, N. Beaulieu, J.D. Youssef, G. Loubens, O. Klein. Appl. Phys. Lett., **118** (3), 032404 (2021). https://doi.org/10.1063/5.0028664
[13] X.R. Wang. Commun. Phys, **4**, 55 (2021). https://doi.org/10.1038/s42005-021-00557-9
[14] L. Huang, Y. Zhou, H. Qiu, H. Bai, C. Chen, W. Yu, L. Liao, T. Guo, F. Pan, B. Jin, C. Song. Adv. Mater., **34** (42), 2205988 (2022). DOI: 10.1002/adma.202205988
[15] O.Y. Arkhipova, A.A. Matveev, A.R. Safin, S.A. Nikitov. Pis'ma v ZhTF **51**, 5 (53) (in Russian). DOI: 10.61011/PJTF.2025.05.59906.20076
[16] A. Hirohata, K. Yamada, Y. Nakatani, P. Ioan-Lucian, B. Dieny, P. Pirro, B. Hillebrands. J. Magn. Magn. Mater., **509**, 166711 (2020). https://doi.org/10.1016/j.jmmm.2020.166711
[17] F. Yang, P.C. Hammel. J. Phys. D: Appl. Phys., **51** (25), 253001 (2018). DOI: 10.1088/1361-6463/aac249
[18] M.I. Dyakonov, V.I. Perel. Phys. Lett. A, **35**, 459 (1971). https://doi.org/10.1016/0375-9601(71)90196-4
[19] E.G. Tveten, A. Brataas, Y. Tserkovnyak. Phys. Rev. B, **92** (18), 80412 (2015). DOI: 10.1103/PhysRevB.92.180412
[20] X. Jia, K. Liu, K. Xia, G.E.W. Bauer. Europhys. Lett., **96**, 17005 (2011). DOI: 10.1209/0295-5075/96/17005
[21] A.B. Cahaya, A.O. Leon, G.E.W. Bauer. Phys. Rev. B, **96**, 144434 (2017). DOI: 10.1103/PhysRevB.96.144434
[22] H. Yuasa, K. Tamae, N. Onizuka. AIP Adv., **7**, 055928 (2017). https://doi.org/10.1063/1.4977496
[23] M.E. Seleznev, Yu.V. Nikulin, S.L. Vysotsky, Yu.V. Khivintsev, A.V. Kozhevnikov, V.K. Sakharov, Y.A. Filimonov. *International symposium „Spin Waves 2024"* (Saratov, Russia, August 26−29, P-44, 2024), https://spinwaves.sgu.ru/index.html
[24] M.E. Seleznev, S.L.Vysotsky, G.M.Amakhanov, Yu.V.Nikulin. *XXIX Mezhdunarodny simpozium „Nanofizika i nanoelektronika"* (10−14 marta 2025, Nizhny Novgorod, 129, 2025),(in Russian) https://nanosymp.ru/ru/archive
[25] S.L. Vysotsky, G.T. Kazakov, A.V. Maryakhin, Yu.A. Filimonov, A.S. He. FTT, **34**, (5), 1376 (1992). (in Russian).
[26] S.L.Vysotsky, M.E.Seleznev, G.M.Amakhanov, Yu.V.Nikulin. Izv. Sarat. un-ta. Nov. Ser. Ser. Fizika, **25** (1), 44 (2025) (in Russian). https://doi.org/10.18500/1817-3020-2025-25-1-44-52

[27] S.L. Vysotsky, G.T. Kazakov, A.V. Maryakhin, Yu.A. Filimonov, A.S. He. RE **35**, 5 (959) (in Russian).
[28] S.L. Vysotskii, M.E. Seleznev, Yu.V. Nikulin, A.V. Kozhevnikov1, G.M. Amahanov, A.G. Timiryazev. Physics of the Solid State, **66** (7), 1023 (2024). DOI: 10.61011/PSS.2024.07.58970.34HH
[29] A.G. Gurevich, G.A. Melkov. *Magnetization Oscillations and Waves* (CRC Press, London, 2020), 464 p. https://doi.org/10.1201/9780138748487
[30] M.E. Seleznev, Y.V. Nikulin, Y.V. Khivintsev, S.L. Vysotskii, A.V. Kozhevnikov, V.K. Sakharov, G.M. Dudko, Y.A. Filimonov. Izvestiya VUZ. Applied Nonlinear Dynamics, **31** (2), 225 (2023). DOI: 10.18500/0869-6632-00303
[31] Yu.V. Nikulin, Yu.V. Khivintsev, M.E. Seleznev, S.L. Vysotskii, V.K. Sakharov, A.V. Kozhevnikov, G.M. Dudko, A.G. Khitun, S.A. Nikitov, Yu.A. Filimonov. J. Exp. Theor. Phys. Lett., **119** (9), 688 (2024). DOI: 10.1134/S0021364024600502
[32] V.S. L'vov, *Nelineynye spinovye volny* (Nauka, M., 1987), 272 s. (in Russian).
[33] A.G. Temiryazev. FTT **29**, 2 (313). (in Russian).
[34] H. Kurebayashi, O. Dzyapko, V.E. Demidov, D. Fang, A.J. Ferguson, S.O. Demokritov. Nature Mater., **10** (9), 660 (2011). DOI: 10.1038/nmat3053
[35] H. Kurebayashi, O. Dzyapko, V.E. Demidov, D. Fang, A.J. Ferguson, S.O. Demokritov. Appl. Phys. Lett., **99** (16), 162502 (2011). DOI: 10.1063/1.3652911
[36] H. Sakimura, T. Tashiro, K. Ando. Nat. Commun., **5**, 5730 (2014). DOI: 10.1038/ncomms6730
[37] G.M. Amakhanov, M.E. Seleznev, Y.V. Nikulin, S.L. Vysotsky, V.K. Sakharov, G.M. Dudko, A.V. Kozhevnikov, Y.V. Khivintsev, Y.A. Filimonov. Izv. vuzov. Radiofizika, **2** (167), 2025 (2009) (in Russian). DOI: 10.52452/00213462_2025_68_02_167
[38] Ch. Kittel. *Introduction to solid state physics* (NY., London, Sydney, Toronto
[39] G.T. Kazakov, A.G. Sukharev, Yu.A. Filimonov. FTT **32**, 12 (3571). (in Russian).
[40] S.A. Kirov, A.I. Pilschikov, N.E. Syriev. FTT **16**, 10 (3051) (in Russian).
[41] S.A. Vyzulin, S.A. Kirov, N.E. Syriev. RE **30**, 1 (179) (in Russian).
[42] A.V. Vashkovsky, E.G. Lokk, V.I. Shcheglov. FTT **41** 11 (2034) (in Russian).

Translated by E.Ilyinskaya